Efficiency-Corrected Yields of $K\Lambda_{1520}$ Channel in Search of High-Mass Nucleon Resonances

Rebecca Osar

Thesis Committee: Michael Dugger (Chair), Barry Ritchie

Arizona State University

Jefferson Lab

April 5, 2023

Abstract

In nuclear physics, there is a discrepancy between theory and experiment concerning the number of existing nucleon resonances. Current models predict far more states than have been observed. In particular, few searches have found excited nucleon resonances in energy ranges over 2.2 GeV in the $K\Lambda$ channel. To investigate this problem, efficiency-corrected yields of the reaction $ep \rightarrow eK^+\Lambda_{1520} \rightarrow eK^+K^-p$ in the center-of-mass energy range 2.1–4.5 GeV are constructed utilizing Jefferson Lab's CLAS12 detector. This paper presents the results of the analysis in the search for high-mass nucleon resonances in the $K\Lambda$ channel between 2.1–4.5 GeV.

Contents

1 Introduction

1.1 Particle Physics Background

The Standard Model relates fundamental particles of matter and force within the universe. The elementary particles are divided into two groups: fermions and bosons. Quarks and leptons are fermions, and they make up the visible matter in the universe. They interact via forces mediated by the bosons shown in Fig. 1.

All electrically charged particles interact electromagnetically via photons. In addition to electric charge, quarks have color charge that dictates interactions via the strong force, which is mediated by gluons. Quarks are never observed alone; due to the property of color confinement, quarks are always bound in colorless combinations, called hadrons. They are most commonly contained in quark-antiquark pairs (mesons) or triplets (baryons), but there are other possible combinations, referred to as exotic hadrons.

While the Standard Model does an excellent job at describing elementary particles, simplifications are required to describe complex interactions. Quantum Chromodynamics (QCD) describes the strong force and its interactions. However, for any bound hadronic system, the predictions calculated from QCD are not consistent with observations. Theorists created models inspired by QCD to predict the allowed masses of baryons by constraining QCD's symmetries and degrees of freedom. One important discrepancy between QCD-inspired models and experimental observations is the "missing resonance" problem.

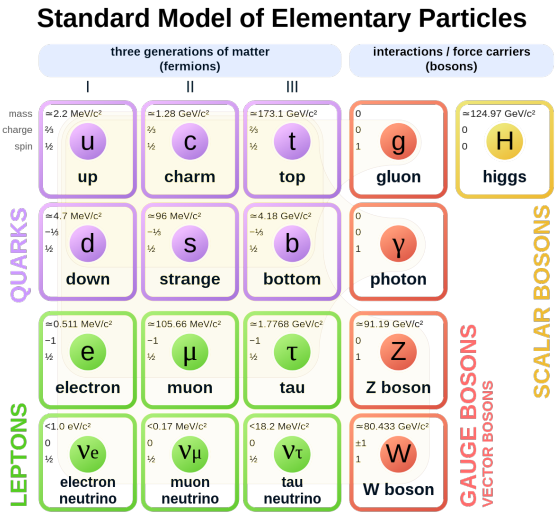

Figure 1: The particles of the Standard Model. Fermions are shown on the left under the three generations of matter; force-carrying bosons are listed on the right in orange and yellow.

1.2 Motivation: Missing Resonances

Particles can be described as stable or unstable, depending on whether they decay spontaneously. Unstable particles are usually particles that have been excited by absorbing energy, either by absorbing photons or being produced in a high-energy collision. Unstable particles may also be produced from decays. Unstable particles decay after a short time; in collider experiments, they can decay in flight prior to hitting detectors. If all the final-state particles are detected, their energy-momentum 4-vectors can be determined and used to reconstruct the parent particle. With large quantities of data, a histogram of the invariant mass of the system will reveal a peak at the mass of the particle—or *resonance*—that decayed. A resonant peak follows a Bright-Wigner distribution with a width inversely proportional to its lifetime due to the energy-time uncertainty principle. A resonant peak reconstructed from a reaction can indicate the existence of a resonance.

The missing resonance problem refers to the discrepancy between the number of predicted excited particle states in certain reactions—or *channels*—and the number of excited particle states that have been observed. Capstick's 1992 review noted eleven predicted excited nucleon (proton or neutron) states that have not been observed in the $N\pi$ channel [2]. Furthermore, Captstick and Roberts' model from 1998 predicted at least 45 nucleon resonances that could decay into $K\Lambda_{1520}$, but only 11 have been observed in the $K\Lambda$ channel [3]. A review by He and Chen from 2012 on the $K\Lambda_{1520}$ channel incorporated effects of resonances near 2080 and 2390 MeV described in Capstick's 1998 review that have not been observed [4]. The discrepancy between theory and experiment points towards potential flaws in our current models and/or experimental techniques. Analyses of experimental data seeking to unearth resonances in specific channels assist in building a more complete collection of experimental results and can provide insight into areas for improvement.

One channel in which missing resonances may be investigated is the $K\Lambda_{1520}$ channel, where an excited nucleon decays into a positive kaon (K^+) and an excited Lambda baryon (Λ_{1520}), which decays into a negative kaon (K^-) and a proton (p). Using data from Jefferson Lab's CLAS12 detector with final state particles eK^+K^-p, a strong signal for the excited Lambda at 1520 MeV (Λ_{1520}) can be reconstructed from the K^-p, as shown in Fig. 3. The $K^+\Lambda_{1520}$ events can be isolated from the background to reveal the resonance spectrum of the whole system. CLAS12 uses an electron beam incident on a proton target, so if a Λ_{1520} in this data were created from a nucleon resonance, it would be produced from the reaction

$$\begin{aligned} ep &\rightarrow eN^* \\ &\hookrightarrow K^+\Lambda_{1520} \\ &\qquad \hookrightarrow K^-p \end{aligned} \tag{1}$$

Here, N^* represents an excited proton. This reaction is illustrated in Fig. 2. By isolating the Λ_{1520} and K^+ system, the resonance spectrum of the system can be studied to look for an excited

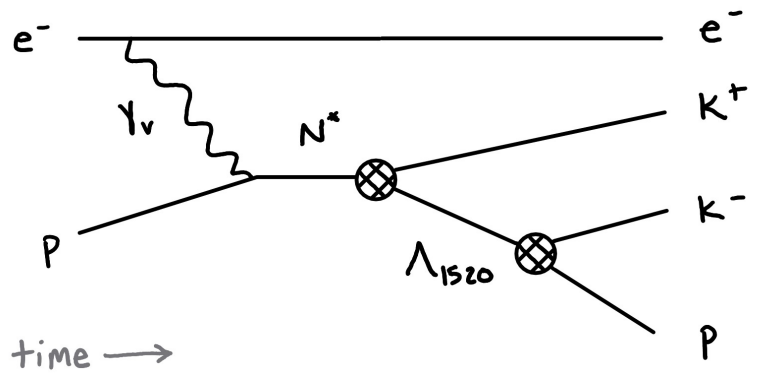

Figure 2: Feynman diagram of the reaction in Eq. 1.

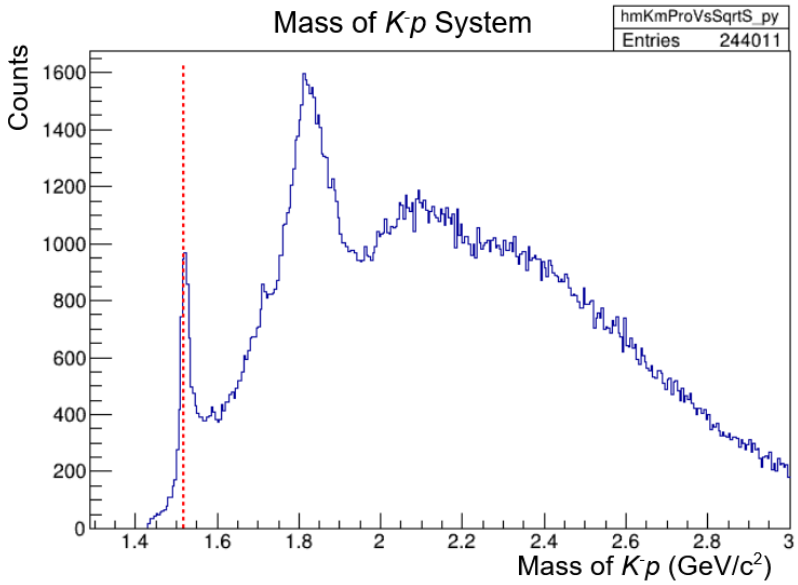

Figure 3: Invariant mass of the K^-p System. The red line at 1.52 GeV/c^2 indicates the Λ_{1520} resonance.

nucleon resonance.

If the Λ_{1520} were not created from a resonance, it would likely be created through a t-channel reaction, where the virtual photon shares a vertex with the K^+ and interacts with the proton via a virtual particle such as a K^-, as depicted in Fig. 4.

In the CLAS12 experiment, the $K\Lambda_{1520}$ reactions in the data used from JLab[1] have a center-of-mass energy W between 2.1–4.5 GeV, which is a range not heavily documented in the Particle Data Group (PDG) records [1]. Investigating this region provides an opportunity to shed light on the resonance spectrum in a channel and energy range that may require more study.

[1]Run Group A (RGA) fall 2018 negative and positive inbending

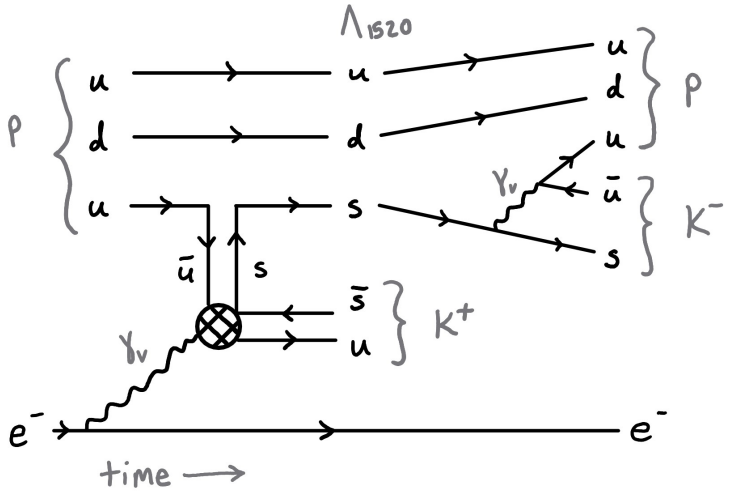

Figure 4: Diagram of t-channel reaction. A $K^+\Lambda_{1520}$ would be produced with no N^*.

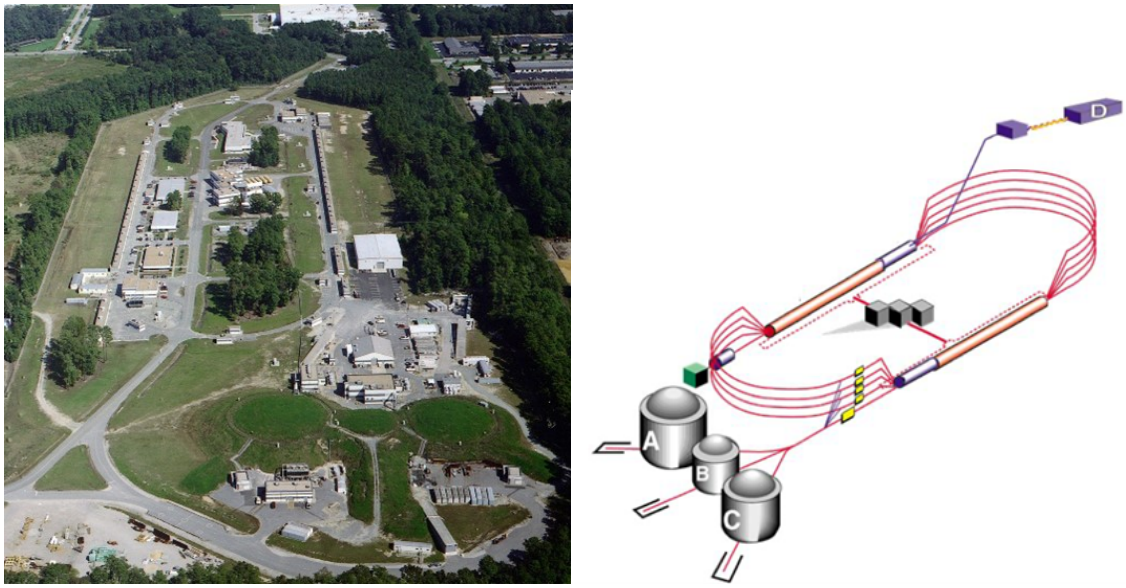

Figure 5: JLab facilities and hall placement around the accelerator

2 Laboratory Facilities

2.1 Thomas Jefferson National Accelerator Facility (JLab)

The Thomas Jefferson National Accelerator Facility (JLab) is a nationally funded lab in Virginia dedicated to studying the structure of nuclear matter. It has an electron accelerator in a racetrack design, and the electron beam may be directed into different halls. There are four halls containing detectors: A, B, C, and D, which are attached to the accelerator as shown in Fig. 5. Hall B studies nuclear interactions using an electron beam at 11 GeV incident on a liquid hydrogen or deuterium target. The detector in Hall B is CLAS12.

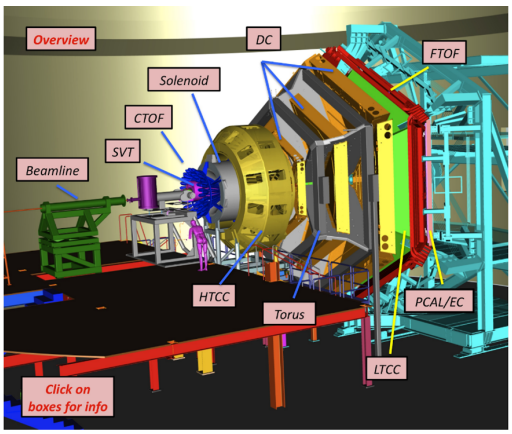

Figure 6: Overview of the CLAS12 detector

2.2 CLAS12 Detector

The detector (Fig. 6) is composed of two main parts: the central detector, located around the target site, and the forward detector, about seven meters downstream of the target. The central detector measures particles in the region $35^\circ < \theta < 125^\circ$ and approximately the full azimuthal range $0 < \phi < 2\pi$, while the forward detector generally measures $5^\circ < \theta < 35^\circ$ and azimuthal angle ϕ coverage ranging from 50% at $\theta = 5^\circ$ to 85% at $\theta = 35^\circ$. The forward detector elements are divided into six equal-sized triangular modules, as shown in Fig. 11.

2.2.1 Beam and Target

Jefferson Lab's CLAS12 detector uses an electron beam of up to 11 GeV and a proton target of liquid hydrogen or deuterium. The beam and target reach a center-of-mass energy of 4.6 GeV.

2.2.2 Tracker and Solenoid

The tracker (Fig. 7), located in the central detector, uses silicon sensors to measure the momentum to determine the vertex position of charged particles. The tracker is designed to operate at a luminosity of 10^{35} $\mathrm{cm}^{-2}\mathrm{s}^{-1}$ and have a momentum resolution of about 6%. The solenoid provides a magnetic field of 5 T along the beamline to allow the tracker to measure the momentum of charged particles. The solenoid can also provide polarization to the target.

2.2.3 Drift Chambers

In the forward detector, there are several drift chamber units (Fig. 8), which are used to measure the momentum of charged particles, similar to the tracker in the central detector. The drift chambers

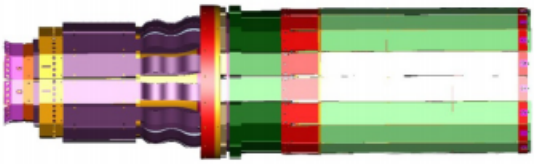

Figure 7: Computer model of the tracker.

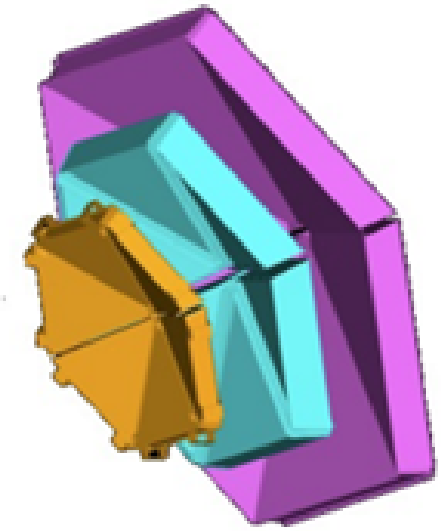

Figure 8: Computer model of the three-part drift chambers.

are equipped with wire sensors and can operate at a luminosity of 10^{35} $\text{cm}^{-2}\text{s}^{-1}$ with a spatial resolution of 250-350 μm.

2.2.4 Central and Forward Time-of-Flight Detectors (CTOF/FTOF)

There are two time-of-flight detectors, one located in the central detector (CTOF), and one in the forward detector (FTOF). They are used to precisely measure the time-of-flight of charged particles for the purpose of particle identification of protons, kaons, and pions. The CTOF has a time resolution of 65 ps. The FTOF contains layers of panels with timing resolutions varying between 60-165 ps, depending on the angle θ. Particle identification (PID) specifications are defined by the timing resolution, n standard deviations of the timing resolution, and the momentum of the particle being measured. The CTOF PID is within 3.3 standard deviations for a particle momentum up to 0.64 GeV/c for π/K separation, up to 1.00 GeV/c for K/p separation, and up to 1.25 GeV/c for π/p separation. The FTOF PID is within 4 standard deviations for a particle momentum up to 2.8 GeV/c for π/K separation, up to 4.8 GeV/c for K/p separation, and up to 5.4 GeV/c for π/p separation.

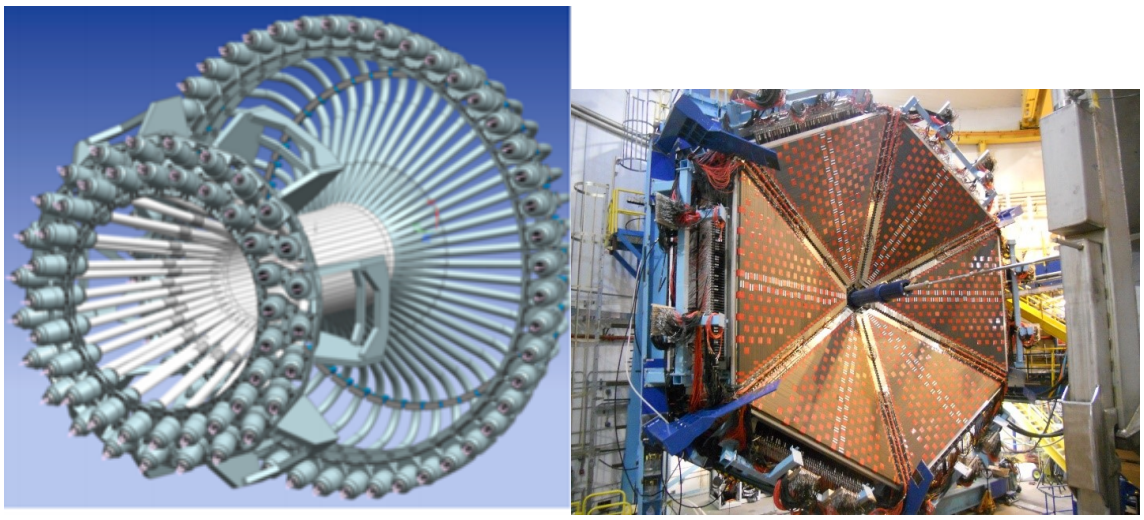

Figure 9: Computer model of the CTOF (left) and FTOF apparatus (right).

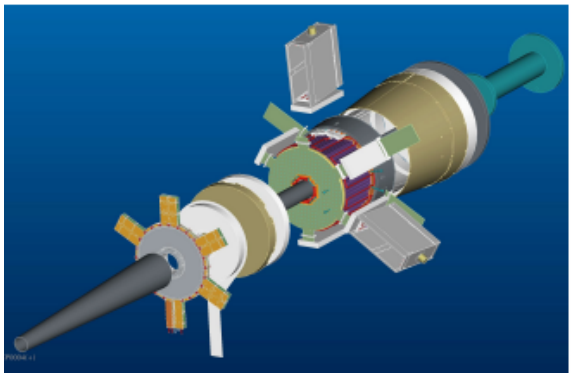

Figure 10: Computer model of the forward tagger

2.2.5 Forward Tagger

The forward tagger (Fig. 10) is used to detect electrons and photons in the range $2.5^\circ < \theta < 4.5^\circ$. The tagger is made up of a homogeneous lead tungstate calorimeter to identify electrons and measure electron energy; a tracker to measure scattering angles; and a scintillation counter to separate electrons and photons. It has an energy resolution of $2\%/\sqrt{E}$, a spatial resolution of 150 μm, and a time resolution of 300 ps.

2.2.6 Electromagnetic and Pre-Shower Calorimeter (ECAL/PCAL)

The forward detector is equipped with an electromagnetic calorimeter (ECAL) and a preshower calorimeter (PCAL) in front, which is used to identify and measure the energy of electrons, photons, $\pi^0 \rightarrow \gamma\gamma$, and neutrons. Both calorimeters (Fig. 11) are made of alternating scintillator strips and lead absorbers. To improve measurements, the orientation of each layer of parallel scintillator strips on the triangular module is rotated 120° from the layer above. The ECAL has an energy

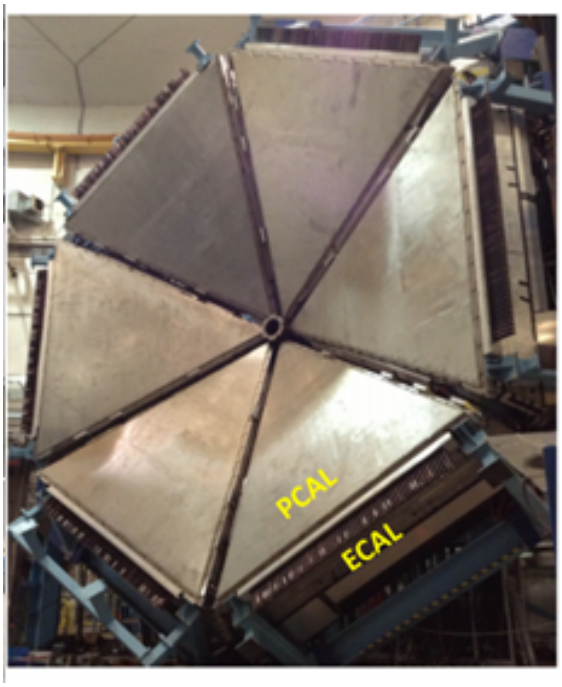

Figure 11: Electromagnetic and pre-shower calorimeter

resolution of $10\%/\sqrt{E}$, position resolution of 5 mm, and timing resolution of 500 ps.

3 Methods

3.1 Acceptance

To select events for the analysis, the datasets were run through selection code to filter out irrelevant or low-resolution data. In the analysis, events with final state particles epK^+K^- were selected. To ensure good resolution, events were only kept if the electron hit the forward tagger, the kaons both hit the forward detector, and the proton hit either the forward or central detectors. Finally, cuts were placed on missing mass, energy, and transverse momentum of the event, three standard deviations from the means. The missing values were calculated from the difference between the 4-momentum of the final state and initial state particle systems. The missing value cuts are shown in Fig. 12.

The missing mass, energy, and transverse momentum cuts removed 91% of the data. Fig. 13 shows a 2D histogram of the mass of the K^-p system vs. the center-of-mass energy W of the final-state particles K^+K^-p before and after the missing value cuts were implemented. Most of the removed events were background at low W near $M_{K^-p} = 1.8$ GeV. Other background was also reduced, while the horizontal signals at $M_{K^-p} = 1.52$ and 1.8 GeV were preserved.

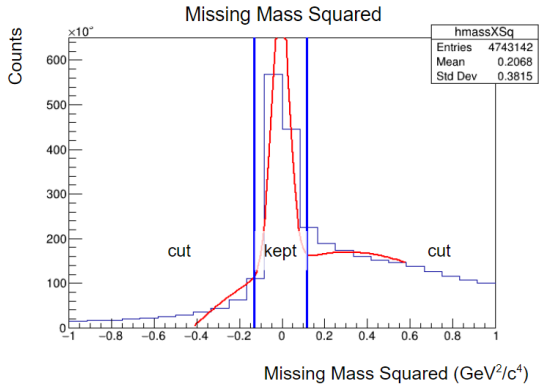

(a) Missing Mass (Squared). The Gaussian has a mean of -0.00741 and a standard deviation of 0.0414; events outside of the bounds -0.132–0.117 GeV were discarded.

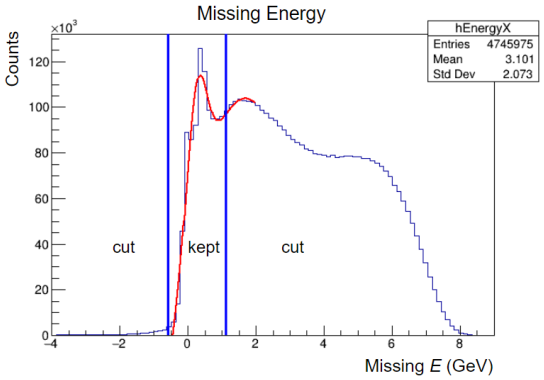

(b) Missing Energy. The Gaussian has a mean of 0.263 and a standard deviation of 0.285; events outside of the bounds -0.591–1.118 GeV were discarded.

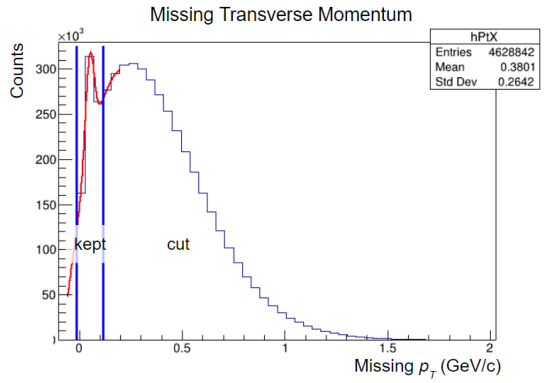

(c) Missing Transverse Momentum. The Gaussian has a mean of 0.0502 and a standard deviation of 0.0213; events outside of the bounds -0.0138–0.114 GeV/c were discarded.

Figure 12: Missing mass (a), energy (b), and transverse momentum (c) cuts. The red line is a Gaussian plus a second degree polynomial fit, where the Gaussian was used to capture the form of the signal and the polynomial fit the background. The blue lines show the bounds three standard deviations from the center of the Gaussian. The data between the bounds were kept; the data outside the bounds were discarded.

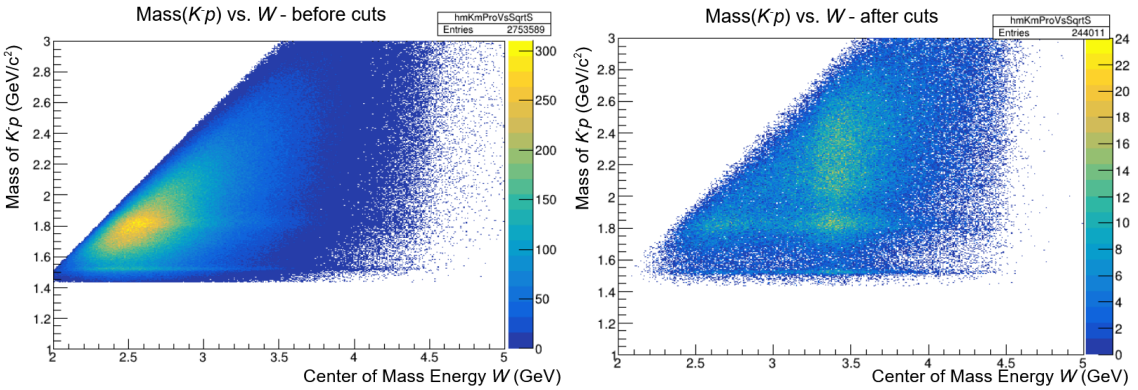

Figure 13: 2D histogram of the mass of the K^-p system (M_{K^-p}) vs. center-of-mass energy of the K^+K^-p system (W) before (left) and after (right) missing value cuts were implemented. The horizontal stripe at 1.52 GeV/c^2 indicates the Λ_{1520} signal.

3.2 Yields

The first step to constructing the resonance spectrum was to find the *yields* of the Λ_{1520} system—that is, the total number of events that decay into a Λ_{1520}—as a function of W. The nucleon resonance was expected to decay into all the final state particles except the electron, so W would be the same center-of-mass energy as the resonance. The Λ, being an unstable particle, was reconstructed from the invariant mass of the K^-p system. Plotting these two values, M_{K^-p} vs. W (Fig. 13), provides insight into the kinematics of the reaction.

To find the Λ_{1520} yields, the signal from the resonance was extracted from the background. Visual demonstrations of this extraction are shown in Fig. 14 and 15. First, only data within the K^-p mass range of 1480-1600 MeV was used. The x-axis of Fig. 13 was divided into bins 60 MeV wide and projected onto the y-axis. The projection gave the mass spectrum of the K^-p system for each W range (Fig. 14). A second-order polynomial plus a Gaussian function was fit onto the total distribution (Fig. 15). The polynomial function fit the background and was subtracted from the total to give the signal. Summing the signal within three standard deviations of the Gaussian mean gave the yield for that W range. Each bin's yield was plotted against W to give the resonance spectrum decaying into $K^+\Lambda_{1520}$. Peaks in this spectrum might indicate the existence of a nucleon resonance that decayed into a $K^+\Lambda_{1520}$.

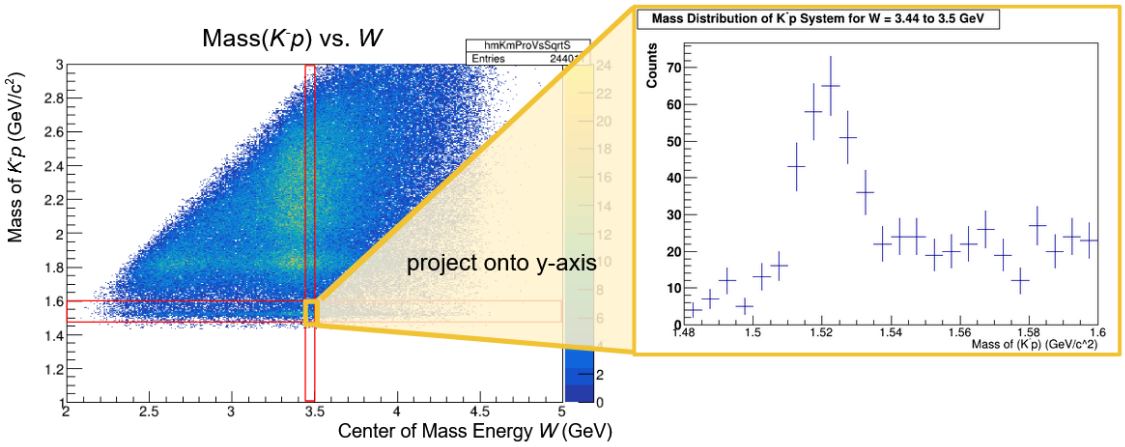

Figure 14: The x-axis of Fig. 13 was divided into bins 60 MeV wide (left). Each bin was projected onto the y-axis in the M_{K^-p} region between 1.48–1.6 GeV/c^2 (right).

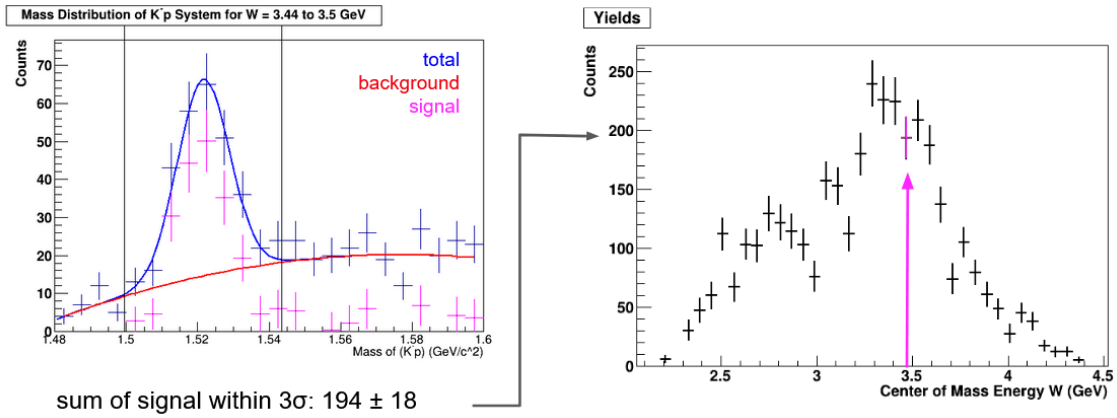

Figure 15: The total mass distribution of the bin (left) was fit with a Gaussian plus a second-order polynomial (blue). The polynomial (red) was subtracted from the total to extract the signal (pink). Two vertical bars show the bounds $\pm 3\sigma$ from the center of the Gaussian. The signal between the bars was summed to give the yield of the bin. The yield was then plotted as a function of W (right).

3.3 Difficulties in Yield Extraction

One source of systematic error in the analysis was the yield extraction fitting routine. The yields were extracted using code that automatically fit the data with a Gaussian plus a second-order polynomial after initializing the mean and width of the Gaussian. To help ensure consistent background fits, the leading coefficient of the background polynomial was constrained to be less than or equal to zero. Every bin was manually inspected for consistency and accuracy. Bins with poor fits were manually readjusted.

For bins with very low statistics, the yields were sometimes over- or underestimated. If the bin could not be fixed manually and appeared to be mostly background with little to no signal, the yield and error were set to zero. An example of a low-statistics bin set to zero is shown in Fig. 16. No bins within $2.4 < W < 4.0$ GeV were set to zero.

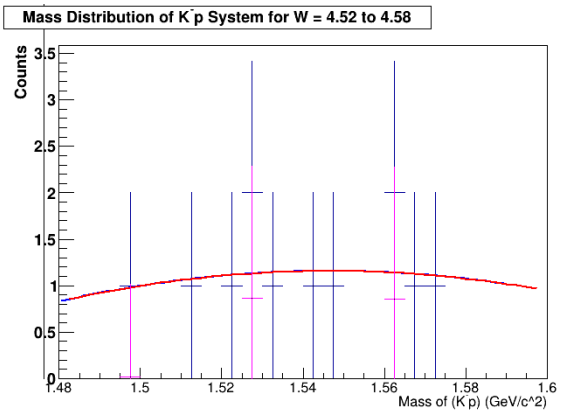

Figure 16: An example of a low-statistics bin that was manually set to zero.

3.4 Efficiency and Acceptance Correction

In the analysis, several corrections were made to the yields. Since the detector efficiencies and acceptance can cause features in the resonance spectrum resembling peaks that are an artifact of the methodology, the yields were efficiency- and acceptance-corrected. The detector efficiency refers to the number of events detected by the CLAS12 detector divided by the total number of events that took place. Acceptance refers to the number of events accepted by the selection code divided by the number of events input. Monte Carlo (MC) simulated data was used to correct the data for efficiency and acceptance.

To create MC data, an event generator was built to simulate the nucleon resonance reaction described in Eq. 1. The generated events were pushed through JLab's MC simulation framework (GEMC) to extract important information about the particles' properties. The output of the GEMC stage was then run through JLab's MC reconstruction framework to simulate which events would be recorded by the detector. Finally, the reconstructed events were pushed through the selection code to make cuts and construct plots.

To correct the data, a histogram of the efficiency as a function of center-of-mass energy W of the K^+K^-p system was constructed. Dividing the reconstructed data histogram (reco) by the generated data histogram (gen) gave the detector efficiency as a function of W. Dividing the histogram of the reconstructed data that went through the selection code (reco cut) by the histogram of the reconstructed data (reco) gave the acceptance. The real data should be divided by these two corrections: efficiency $\left(\frac{\text{reco}}{\text{gen}}\right)$ and acceptance $\left(\frac{\text{reco cut}}{\text{reco}}\right)$. Multiplying these terms together, the reco's cancel out, and the total correction becomes $\frac{\text{reco cut}}{\text{gen}}$. In this experiment, the data was divided by this ratio as a function of W to correct for efficiency and acceptance.

3.5 A Note on Datasets

The experiment used two datasets from JLab: Run Group A (RGA) fall 2018 positive inbending and negative inbending. Negative inbending means negative particles were bent towards the beampipe and positive particles were bent away from the beampipe. The datasets were labeled Fa18Pos and Fa18Neg, respectively. For the main analysis, the datasets were combined before implementing the yield extraction code. This method improved the statistics in the bins, which improved the consistency and accuracy of the fitting routine. The efficiencies of the two datasets

were added, scaled by the number of events in each dataset. The total yields were divided by the total efficiencies to obtain efficiency-corrected yields.

4 Results

4.1 Combined Data

The efficiencies of the combined 2018 data obtained from the generated and reconstructed MC simulated data are shown in Fig. 17. High volumes of low-energy thrown events combined with few low-energy seen events caused extremely low efficiencies at low energies.

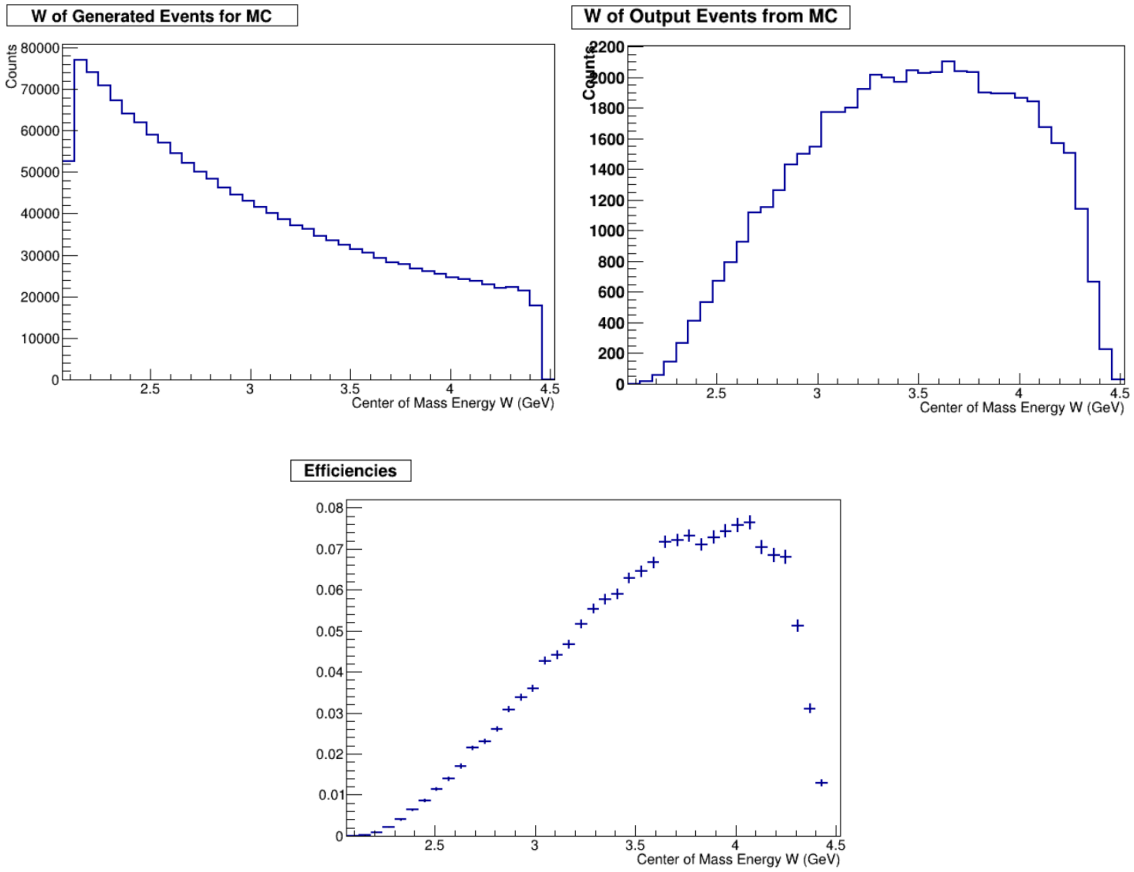

Figure 17: Generated events (top left), reconstructed events passed through selection (top right), and efficiencies (bottom) as a function of center-of-mass energy W from the 2018 combined data. The generated events were "thrown" events; the events that made it through both reconstruction and the selection code were "seen" events. The efficiencies were obtained by dividing "seen" by "thrown" events.

The yields and corrected yields of the combined 2018 data are shown in Fig. 18. The low efficiencies and low statistics in the yields at low energies caused very large error bars at low energies in the corrected yields. Consequently, the corrected yields are difficult to analyze at low energies.

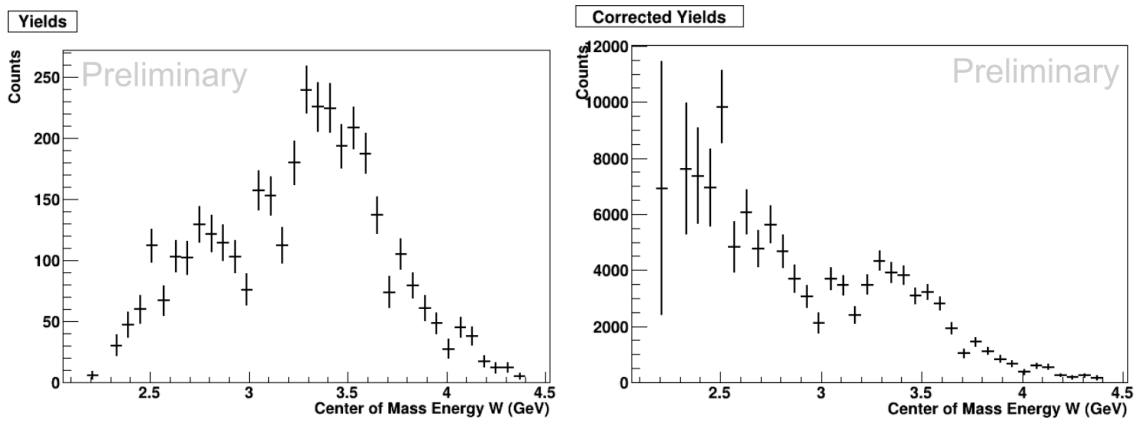

Figure 18: Yields (left) and efficiency-corrected yields (right) of the 2018 combined data. After correction, the spectrum exhibits features around 3.1 and 3.3 GeV.

4.2 Individual Datasets

The corrected yields of the individual 2018 datasets were also explored to investigate similarities or discrepancies compared to the combined data. The individual efficiency-corrected yields were plotted superimposed on a canvas and are shown in Fig. 19.

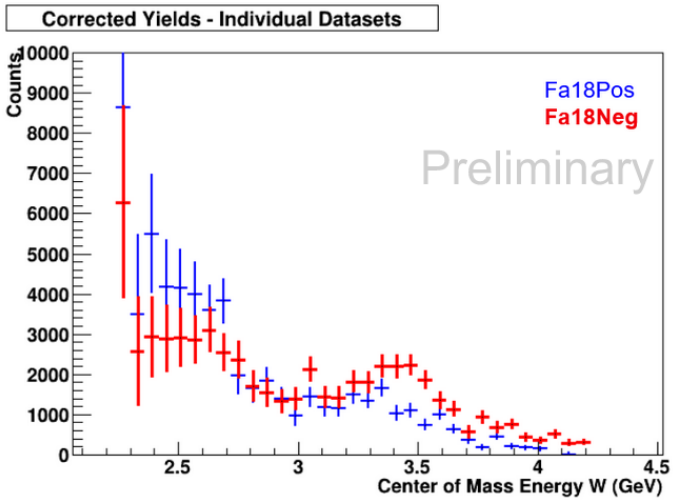

Figure 19: Efficiency-corrected yields of the 2018 positive and negative inbending datasets, respectively. A narrow feature exists near 3.1 GeV. A discrepancy between the datasets in the 3.4–3.6 GeV range requires further study.

5 Discussion

5.1 The Resonance Spectrum

Two features appeared in the resonance spectrum of the combined 2018 data. While the bumps at 3.1 and 3.3 GeV were outside the error of neighboring data points, other systematics in the

experiment could affect the shape of the spectrum and the reliability of the results. Further study is required to investigate the nature of the features and the way systematics impact the shape of the resonance spectrum. Improving statistics by using different data in the analysis and adjusting the fitting routine can provide insight into the shape of the spectrum. If improved or adjusted methodology removes or changes the bumps, they were not resonances. From this analysis, no definitive resonances were discovered.

5.2 RGA Spring 2019 Dataset

In the analysis, statistics were attempted to be improved by incorporating JLab's RGA spring 2019 data. During the individual dataset analysis, a large discrepancy was revealed between 2.9–3.3 GeV in the 2019 corrected yields spectrum. The CLAS12 collaboration recently released the second pass of the 2019 spring RGA data and recommended all analyses using the data be reanalyzed. Due to time constraints, the spring 2019 data was omitted entirely from the analysis. Future studies should investigate the newly cooked data to explore its reliability and use in a nucleon resonance search.

6 Conclusions

There are two features in the resonance spectrum at 3.1 and 3.3 GeV that require further study. From this search, no definitive nucleon resonances were found. Future steps for the analysis include refining the yield extraction code and exploring the newly cooked RGA spring 2019 data.

References

[1] V. Burkert, E. Klempt, U. Thoma, L. Tiator, and R. Workman. N and δ resonances. Revised 2019.

[2] S. Capstick. Photo- and electroproduction of nonstrange baryon resonances in the relativized quark model. *Physical Review D*, 46(7), 1992.

[3] S. Capstick and W. Roberts. Strange decays of nonstrange baryons. *Physical Review D*, 58, 1998.

[4] J. He and X. Chen. Roles of nucleon resonances in $\lambda(1520)$ photoproduction off the proton. *Physical Review C*, 86, 2012.